Hindawi
Wireless Communications and Mobile Computing
Volume 2023, Article ID 9814786, 1 page
https://doi.org/10.1155/2023/9814786

Retraction

Retracted: Sidelobe Reduction in NC-OFDM-Based CRNs Using Differential Evolution-Assisted Generalized Sidelobe Canceller

Wireless Communications and Mobile Computing

Received 12 December 2023; Accepted 12 December 2023; Published 13 December 2023

This article has been retracted by Hindawi, as publisher, following an investigation undertaken by the publisher [1]. This investigation has uncovered evidence of systematic manipulation of the publication and peer-review process. We cannot, therefore, vouch for the reliability or integrity of this article.

Please note that this notice is intended solely to alert readers that the peer-review process of this article has been compromised.

Wiley and Hindawi regret that the usual quality checks did not identify these issues before publication and have since put additional measures in place to safeguard research integrity.

We wish to credit our Research Integrity and Research Publishing teams and anonymous and named external researchers and research integrity experts for contributing to this investigation.

The corresponding author, as the representative of all authors, has been given the opportunity to register their agreement or disagreement to this retraction. We have kept a record of any response received.

References

[1] R. Ahmed, N. Gul, S. Ahmed, M. S. Khan, S. M. Kim, and J. Kim, "Sidelobe Reduction in NC-OFDM-Based CRNs Using Differential Evolution-Assisted Generalized Sidelobe Canceller," *Wireless Communications and Mobile Computing*, vol. 2022, Article ID 9449400, 11 pages, 2022.

Hindawi
Wireless Communications and Mobile Computing
Volume 2022, Article ID 9449400, 11 pages
https://doi.org/10.1155/2022/9449400

Research Article

Sidelobe Reduction in NC-OFDM-Based CRNs Using Differential Evolution-Assisted Generalized Sidelobe Canceller

Rashid Ahmed,[1] **Noor Gul**,[1,2] **Saeed Ahmed**,[2] **Muhammad Sajjad Khan**,[3] **Su Min Kim**,[2] **and Junsu Kim**[2]

[1]*Department of Electronics, University of Peshawar, Peshawar 25000, Pakistan*
[2]*Department of Electronics Engineering, Tech University of Korea (TU Korea), Republic of Korea*
[3]*Department of Electrical Engineering, Faculty of Engineering and Technology, International Islamic University, Islamabad 44000, Pakistan*

Correspondence should be addressed to Junsu Kim; junsukim@kpu.ac.kr

Received 1 October 2021; Revised 24 January 2022; Accepted 14 March 2022; Published 4 April 2022

Academic Editor: Ali Kashif Bashir

Noncontiguous orthogonal frequency division multiplexing (NC-OFDM) is considered a suitable candidate for the cognitive radio network (CRN) to accomplish efficient data transmission. The NC-OFDM allows secondary users (SUs) to access the primary user (PU) spectrum while being detected idle. However, interference may occur in the adjacent frequency bands of the PU due to sidelobes of the SU transmission. The use of cancellation carriers (CCs) and generalized sidelobe canceller (GSC) is a widely adopted technique to tackle the sidelobes. To this end, this paper presents a differential evolution- (DE-) based GSC (DE-GSC) scheme to suppress unwanted sidelobes. At first, in the DE-GSC1 scheme, the adaptive weight vector is calculated using the DE algorithm while considering the complete samples of the sidelobes for optimization. The optimized weights are then added with the original weights to reduce the sidelobe issue. Next, in the DE-GSC2 scheme, selected elements for the adaptive weight vector near the main NC-OFDM signal are computed using the DE to reduce the search space. The performance of the proposed methods in terms of power spectral density (PSD) is compared with some of the recent techniques employing five different scenarios. Simulation results in the presence of single and multiple spectral hole scenarios validate that the proposed DE-GSC1 and DE-GSC2 methods result in enhanced suppression performance compared with the: original signal, simple CC, simple GSC, DE-based CC (DE-CC), and genetic algorithm- (GA-) based CC (GA-CC) schemes.

1. Introduction

The radio spectrum demand is rising with the increase in the number of wireless devices and services. The spectrum estimation surveys show that most spectrum bands are underutilized most of the time [1]. A progressively adaptable spectrum managing approach is required to solve the spectrum underutilization problems. Several ideas regarding adaptive spectrum management exist such as dynamic sharing of the spectrum. Therefore, the administrative bodies have started reconsidering the static spectrum access to shift towards dynamic spectrum access.

The cognitive radio network (CRN) allows secondary users (SUs) to opportunistically access spectrum resources using its detection, learning, and intelligence features [2]. The major problem in CRN occurs when a SU accesses a licensed band but fails to notice the existence of the primary user (PU), causing interference [3]. Hence, the responsibility of the interference management mostly depends on the SUs.

In the interweave mode of CRN, SUs are allowed to opportunistically access the spectrum based on noninterference to the PUs [3–6]. To detect the occupancy of the PU spectrum, commonly used detection schemes adopted by the SUs are the generalized likelihood ratio test detector

(GLRT), matched filter detector (MFD), feature detector, and energy detectors [7, 8]. Subsequent measures are required at the transmitter side to control the shape of the transmitted signal; therefore, both the SU and PU can have similar spectrum assets with low interference [6, 9].

Noncontiguous orthogonal frequency division multiplexing (NC-OFDM) is considered the best candidate for CRN [10, 11]. The NC-OFDM transmits signals on narrowband channels reducing the effect of intercarrier interference (ICI) and intersymbol interference (ISI) [12]. It is a multicarrier system that splits the existing overall bandwidth into numerous narrow orthogonal channels/subcarriers. In parallel, NC-OFDM has some downsides due to the existence of the sidelobes that generate high out-of-band (OOB) radiations.

To handle the OOB radiations issue, different strategies are suggested in the time and frequency domains. The time-domain techniques include adaptive symbol transmission [13], filtering [14], and windowing [15, 16], while the frequency-domain incorporates cancellation carrier (CC) insertion [17] and generalized sidelobe canceller (GSC). To reduce the sidelobe issues in the PU regions, the CC scheme employs extra subcarriers, known as CCs at the edges of the OFDM symbol. These CCs do not contribute to the data transmission; however, they consume the extra bandwidth. Therefore, the CCs are considered detrimental. On the contrary, extra subcarriers are not used in the GSC; rather the given NC-OFDM signal is passed through the upper and lower branches of the GSC to suppress the OOB radiations. The GSC is the simplest version of linearly constrained minimum variance (LCMV), where the constrained optimization problem is converted into an unconditional problem.

Some of the schemes to reduce sidelobes power are the subcarrier weighting [18], advanced subcarrier weighting [19], efficient subcarrier weighting [20], insertion of modified CCs using heuristic techniques [9], peak to the average method of suppression constellation adjustment [21], and GSC [22]. The other methods in use are the additive signal method [23], extended active interference cancellation [24], efficient sidelobe suppression technique [25], minimization of sidelobe using modify GSC [26], a mongrel technique to reduce sidelobes [27], multiple generalized sidelobe technique for suppression of sidelobes [28], joint peak to average power ratio (PAPR) reduction technique [29], filter-based sidelobe reduction scheme [30], and hybrid PAPR method [31].

Conventionally, GSC adjusts the weights of the adaptive weight vector using the numerical solution to suppress high OOB radiations. On the other hand, the CC techniques reduce available bandwidth opportunity for the SUs with the insertion of extra CCs. Contrary to the above-mentioned schemes, we employed the differential evolution (DE) to optimize the adaptive weight vector of the GSC as an alternative to the numerical solution to attain improved sidelobe suppression. Major contributions of this paper are listed below:

(i) The DE-based GSC (DE-GSC) scheme is suggested in the paper. We proposed two schemes: DE-GSC1 and DE-GSC2. Both the proposed schemes, DE-GSC1 and DE-GSC2, are modified versions of the simple GSC scheme, where the adaptive portion of the simple GSC is tuned using the DE to get maximum OOB suppression results

(ii) To reduce the sidelobe weights using the DE-GSC1, a considerably large set of values in the adaptive weight vector are optimized through the DE algorithm. Similarly, the DE-GSC2 reduces sidelobe issues in the NC-OFDM by optimizing some of the adaptive weight vector values near the main NC-OFDM signal

(iii) The effectiveness and reliability of the proposed schemes are compared with widely adopted existing schemes, like simple GSC, simple CCs, Brandes-based CCs (Brandes-CC), genetic algorithm- (GA-) based CCs (GA-CCs), and DE-based CCs (DE-CCs). Simulation results for the single and multiple white spaces in five different cases show improved sidelobe concealment performance by the proposed DE-GSC1 and DE-GSC2 as compared with the other schemes

The remaining paper is organized as follows. In Section 2, the system model is discussed. Section 3 gives a detailed description of the proposed scheme. Simulation results are discussed in Section 4. The paper is concluded in Section 5.

2. System Model and Background

2.1. System Model. Consider that K number of SUs is trying to access the PU spectrum in the interweaved mode. We assume that both the PU and the SUs are based on the NC-OFDM. Consider the spectrum band is divided into S subcarriers out of which S_d subcarriers are allocated to the d^{th} SU, such that $S_d \leq S$. These subcarriers are modulated with binary phase-shift keying (BPSK) or quadrature phase-shift keying (QPSK). The baseband NC-OFDM signal for the d^{th} SU in one symbol time-domain duration is

$$x_d(t) = \sum_{n=r}^{S_d-1} p_{n,d} e^{j2\pi f_n t} I(t), \tag{1}$$

where $x_d(t)$ is the NC-OFDM signal of the d^{th} SU, $p_{n,d}$ are the data modulated symbol of the d^{th} SU on the n^{th} subcarrier, r is any arbitrary subcarrier, f_n define the subcarrier frequencies, and $I(t)$ is a rectangular function [32] that can be defined as

$$I(t) = \begin{cases} 1, & T_{\text{gu}} \leq t \leq T_s, \\ 0, & \text{otherwise}, \end{cases} \tag{2}$$

where T_{gu} and T_s are the guard interval length and symbol duration, respectively. The Fourier transform of (1) is given as

$$X_d(f) = \sum_{n=r}^{S_d-1} p_{n,s}\,\mathrm{sinc}\left(\pi(f-f_n)T'\right), \tag{3}$$

where $\mathrm{sinc}(x) = \sin(\pi x)/\pi x$ is the sinc function with symbol duration $T' = T_s + T_{gu}$. The sidelobe power in the frequency domain decays as a function $1/f^2 S_d$ in Figure 1 that results in extreme interference to the PU transmission.

2.2. Generalized Sidelobe Canceler (GSC). The input NC-OFDM signal passes through both the upper and the lower portions of the GSC in Figure 2. The upper portion comprises of quiescent weight vector $\mathbf{w}_q$ constructed by several constraints, to maintain the desired segment of the signal, termed fixed beamformer (FBF), while the lower portion comprises a blocking matrix $\mathbf{B}$ and an adaptive weight vector $\mathbf{w}_a$. The blocking matrix blocks desired segment of the signal and preserves the undesired segment of the signal as in Figure 1.

The adaptive weight vector $\mathbf{w}_a$ then adjusts the weights of the undesired segments that result in the sidelobe reduction when the signals from the upper and the lower portions are subtracted.

To evaluate the expression for $\mathbf{w}_a$, $\mathbf{B}$, and $\mathbf{w}_q$, the NC-OFDM in (3) and Figure 1 is first one sampled into equally spaced C values and collected in vector $\mathbf{v} = [v_1 \quad v_2 \quad \cdots \quad v_C]^T$, where each sample element represents NC-OFDM signal magnitude. This is made with an assumption that all NC-OFDM samples are uncorrelated, which are next passed through the GSC to get the output as

$$Y = \mathbf{w}^H \mathbf{v}, \tag{4}$$

where $\mathbf{w} = [w_1 w_2 \cdots w_C]^T$ is a vector with the size $(C \times 1)$, where H denotes Hermitian. The weight vector $\mathbf{w}^H$ is determined using LCMV [33] that minimizes the output power using multiple linear constraints. The optimization problem of the LCMV is formulated as

$$\begin{aligned} &\min_{w} \quad \mathbf{w}^H \mathbf{R}_v \mathbf{w} \\ &\text{s.t} \quad \mathbf{w}^H \mathbf{J} = \mathbf{g}^H, \end{aligned} \tag{5}$$

where $\mathbf{R}_v = E[\mathbf{v}\mathbf{v}^H] = \sigma^2 \mathbf{I}$ represents a correlation matrix, with $C \times C$ dimension, and $\mathbf{g} = [1 \quad 1 \quad \cdots \quad 1]^T$ is a gain vector with dimension $N \times 1$ consisting of desired gain associated with each steering vector. Similarly, $\mathbf{I}$ represents an identity matrix with $C \times C$ dimension, σ^2 denotes the variance, and $\mathbf{J}$ shows the constraint matrix with the size $C \times N$.

After solving (5) using Lagrange's multipliers, we get

$$l = \mathbf{w}^H \mathbf{R}_v \mathbf{w} + \left(\mathbf{w}^H \mathbf{J} - \mathbf{g}^H\right)\lambda + \lambda^H \left(\mathbf{J}^H \mathbf{w} - \mathbf{g}\right), \tag{6}$$

$$\frac{\partial}{\partial \mathbf{w}^H}\left(\mathbf{w}^H \mathbf{R}_v \mathbf{w} + \mathbf{w}^H \mathbf{J}\lambda - \mathbf{g}^H \lambda + \lambda^H \mathbf{J}^H \mathbf{w} - \lambda^H \mathbf{g}\right) = 0, \tag{7}$$

$$\mathbf{w} = -\mathbf{R}_v^{-1} \mathbf{J}\lambda, \tag{8}$$

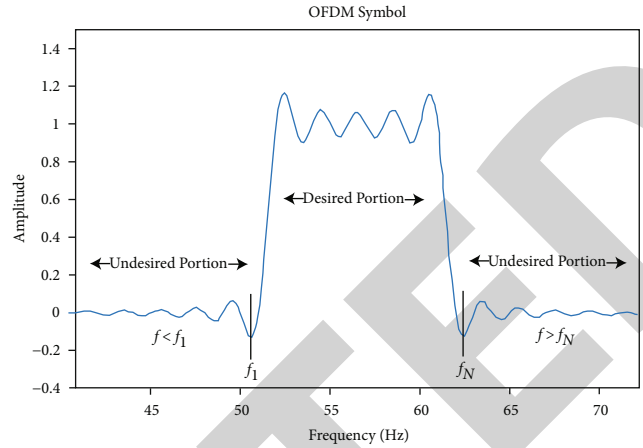

Figure 1: OFDM symbol with high sidelobes.

where λ is the Lagrange multiplier, $(\partial/\partial \mathbf{w}^H)(\mathbf{w}) = 0$ and $(\partial/\partial \mathbf{w}^H)(\mathbf{w}^H) = 1$. Put (8) into the constraint equation $\mathbf{w}^H \mathbf{J} = \mathbf{g}^H$, we get

$$-\lambda^H \mathbf{J}^H \mathbf{R}_v^{-1} \mathbf{J} = \boldsymbol{g}^H. \tag{9}$$

For solving λ, substitute (9) into (8)

$$\mathbf{w}^H = \mathbf{g}^H \left(\mathbf{J}^H \mathbf{R}_v^{-1} \mathbf{J}\right)^{-1} \mathbf{J}^H \mathbf{R}_v^{-1}. \tag{10}$$

The N steering vectors of $\mathbf{J}$ matrix are specified as

$$\mathbf{J} = [\mathbf{s}_1 \quad \mathbf{s}_2 \quad \cdots \quad \mathbf{s}_N], \tag{11}$$

where N is the overall frequency in the desired portion of the signal, as in Figure 1. Similarly, $\mathbf{s}_i = [s_1 \quad s_2 \quad \cdots \quad s_C]^T$ is the i^{th} steering vector that consists of C samples in the i^{th} spectrum bearing $C \times 1$ dimensions.

The employment of LCMV is to split a field with $C \times C$ dimension into the constraint subfield well-defined by the columns of $\mathbf{J}$ $(C \times N)$ the matrix and an orthogonal subfield denoted as $\mathbf{B}$ having dimension $C \times (C - N)$

$$\mathbf{J}^H \mathbf{B} = \mathbf{O}, \tag{12}$$

where $\mathbf{O}$ represents a null matrix with dimension $N \times (C - N)$ and $\mathbf{B}$ symbolizes a blocking matrix that blocks the desired portion of the NC-OFDM signal.

The $\mathbf{B}$ can be determined through singular value decomposition or QR factorization [34]. It is constructed, by first finding $\mathbf{P}_o = \mathbf{I} - \mathbf{P}_c$ with $\mathbf{P}_c$ and $\mathbf{P}_o$ representing matrix projection onto the constraint and orthogonal subfields with $C \times C$ dimension, formerly orthonormalizing$\mathbf{P}_o$ and choosing the first$(C - N)$columns of the orthonormalized matrix to construct a blocking matrix$\mathbf{B}$, having the property [33].

$$\mathbf{B}^H \mathbf{B} = \mathbf{I}. \tag{13}$$

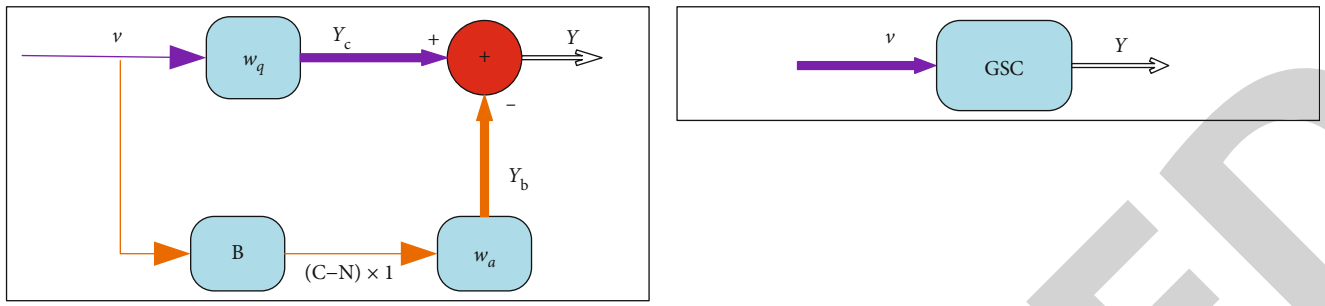

FIGURE 2: Generalized sidelobe canceller (GSC): (a) block diagram of GSC; (b) equivalent block diagram of GSC.

The quiescent weight vector $\mathbf{w}_q^H$ of the GSC is determined as

$$\mathbf{w}_q^H = \mathbf{g}^H \left[\mathbf{J}^H \mathbf{J}\right]^{-1} \mathbf{J}^H. \tag{14}$$

Similarly, the optimal value of the adaptive weight vector is achieved as

$$\mathbf{w}_{a(\text{opt})}^H = \boldsymbol{w}_q^H \mathbf{R}_v \mathbf{B} \left(\mathbf{B}^H \mathbf{R}_v \mathbf{B}\right)^{-1}. \tag{15}$$

Hence, the GSC outcomes in (4) yield

$$Y = \left(\mathbf{w}_q - \mathbf{B}\mathbf{w}_a\right)^H \mathbf{v}. \tag{16}$$

Similarly, the output power of GSC is as

$$P = \left(\mathbf{w}_q - \mathbf{B}\mathbf{w}_a\right)^H \mathbf{R}_v \left(\mathbf{w}_q - \mathbf{B}\mathbf{w}_a\right). \tag{17}$$

The block diagram of GSC with its components is shown in Figure 2.

3. Proposed Sidelobe Cancelation Method

In this section, we present DE-GSC1 and DE-GSC2 as the proposed schemes for sidelobe reduction. The proposed schemes are the modified versions of the conventional GSC that will result in the reduction of sidelobes. In this paper, the optimization portion of GSC, i.e., the adaptive weight vector, is carried out using the DE algorithm.

3.1. Differential Evolution Based Weighting Method. In the proposed DE-GSC1 scheme, all elements of the adaptive weight vector $\mathbf{w}_a$ are optimized using DE. The elements of the adaptive weight vector are selected from both ends of the OFDM sidelobe. To optimize the performance of the proposed DE-GSC 1, the entire vector element from each sidelobe is considered for the reduction of OOB radiation, while in the DE-GSC2 some of the adaptive weight vector elements with high OOB radiation magnitudes near the main OFDM symbol in Figure 1 are determined using the DE algorithm. A total of eight sample elements from each sidelobe are collected for optimization in the DE-GSC2. These weights are the maximum and minimum weights from the sidelobes. The other elements of the adaptive weight vector in the DE-GSC2 are determined using the sidelobe decaying formula. The main steps involved in the DE algorithm to solve the given problem are discussed as follows.

3.1.1. Step 1: Initialize Population. In the first step, the weight vectors to suppress the OOB radiations of the NC-OFDM symbol are initialized randomly with N_p population members (candidate solutions) consisting of D total dimensions.

$$\mathbf{u}_{i,j}^G = h + \text{randj}\left(h_j - l_j\right), \quad i = 1, 2, \cdots, N_p, j = 1, 2, \cdots, D. \tag{18}$$

The vector $\mathbf{u}_{i,j}^G$ in (18) is the target vector, randj is a uniformly distributed random number between (0,1), h_j and l_j are the upper and lower bound limits of the j^{th} decision parameter, respectively. Here, the dimension D is identical to the total number of elements in the adaptive weight vector. The fitness of each of these target vectors is determined in the form of sidelobe suppression, and the vector with minimum OOB radiations is selected.

3.1.2. Step 2: Mutation. For each weight vector in the given population, three dissimilar random numbers b_1, b_2, and b_3 are generated such that they are different from the running index as well. Now, the initial population in (18) and the random numbers b_1, b_2, and b_3 are used to form a new population. The mutation results in the mutant or the donor vector as

$$\mathbf{m}_i^{G+1} = \mathbf{u}_{b1}^G + F\left(\mathbf{u}_{b2}^G - \mathbf{u}_{b3}^G\right), \quad i = 1, 2, 3 \cdots, N_p, b_1 \neq b_2 \neq b_3 \neq i. \tag{19}$$

Here, $\mathbf{m}_i^{G+1}$ is the mutant or mutation vector. The scaling factor F is the tuning parameter and is problem-dependent. It is carefully selected keeping the value of the decision parameter between l_j and h_j to finalize optimum weight vector with minimum sidelobe power. The scaling factor F is selected as 0.2 in the proposed schemes for better sidelobe suppression results. The difference employed in the mutation process in (19) forms the given algorithm as DE.

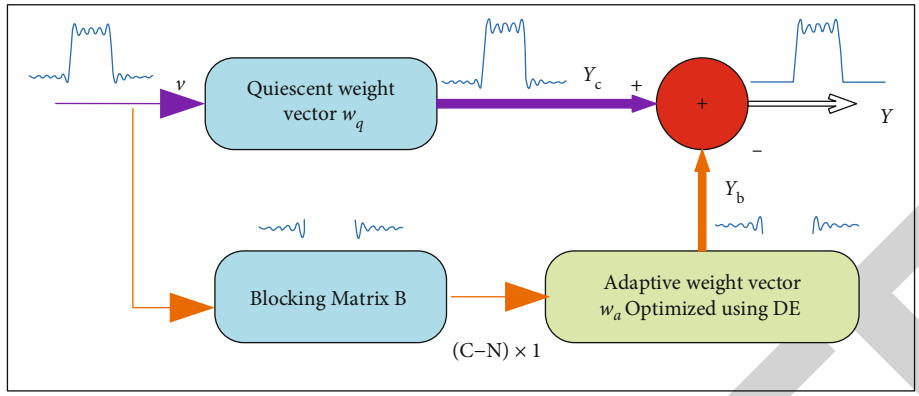

Figure 3: Proposed DE-GSC.

3.1.3. Step 3: Crossover. The crossover is performed between donor and target vectors. The resultant crossover is formed as follows:

$$\mathbf{z}_{i,j}^{G+1} = \begin{cases} \mathbf{m}_{i,j}^{G+1}, & \text{rand } (j) \le \xi \text{ or } j = \text{randn}(i), \\ \mathbf{u}_{i,j}^{G}, & \text{rand } (j) > \xi \text{ or } j \ne \text{randn}(i), \end{cases} \tag{20}$$

where rand $(j) \in [0, 1]$ is the uniformly distributed random number, while j is the element number of the candidate solution; i.e., $j \in 1, 2, \cdots, D$ and -randn(i) is an integer, randomly selected from 1 to D. Similarly, $\mathbf{z}_{i,j}^{G+1}$ is the trial vector, and ξ is the cross-over rate selected (0.9).

3.1.4. Step 4: Selection. In this step, a comparison is made between the trial vector $\mathbf{z}_{i,j}^{G+1}$ and target vector $\mathbf{u}_i^G$ in terms of its fitness. The weight vector with an improved fitness function that shows better sidelobe reduction is selected for the next generation as

$$\mathbf{u}_i^{G+1} = \left\{ \begin{matrix} \mathbf{z}_i^{G+1}, & f\left(\mathbf{z}_i^{G+1}\right) < f\left(\mathbf{u}_i^G\right) \\ \mathbf{u}_i^G, & f\left(\mathbf{z}_i^{G+1}\right) \ge f\left(\mathbf{u}_i^G\right) \end{matrix} \right\}. \tag{21}$$

The vector $\mathbf{u}_i^{G+1}$ is an offspring for the next generation. As the objective of the proposed work is to reduce sidelobe power, hence, it is considered a minimization problem. The sidelobe weights are optimized with DE after several iterations and subtracted from the original weight resulting in the sidelobes suppression as follows:

$$f = |\mathbf{u}_s - \mathbf{u}|. \tag{22}$$

In (22), $\mathbf{u}_s$ is the sidelobe original weights and $\mathbf{u}$ consists of the optimized weight vector using the DE algorithm. The block diagram of the DE-GSC is shown in Figure 3.

A pseudocode of the proposed algorithm that determines the adaptive weight vector of the GSC for reducing sidelobe power due to the SUs transmission is as follows:

```
(1)  Start Differential Evolution
(2)  t = 1
(3)  Initialize-populationu^t = {u_i^t, i = 1, 2, 3 ⋯ , N} ;
(4)  While conditions are not satisfied
(5)    For i=1 to N do
(6)      Randomly select b_1, b_2, b_3 ∈ 1, 2, ⋯N ;
(7)      Randomly select  δ_i ∈ 1, ⋯, n ; .
(8)    For j = 1 to n
(9)      m_{i,j}^{t+1} = u_{b_1}^t + F(u_{b_2}^t − u_{b_3}^t)
(10)   b_1 ≠ b_2 ≠ b_3 ≠ i
(11)   If rand (j) > ξ or j ≠ randn(i)
(12)     z_{i,j}^{t+1} = m_{i,j}^{t+1}
(13)   Else
(14)     z_{i,j}^{t+1} = u_{i,j}^t
(15)   End if
(16)   End For
(17)   If f(z_i^{t+1}) < f(u_i^t)
(18)     u_i^{t+1} = z_i^{t+1}
(19)   Else
(20)     u_i^{t+1} = u_i^t
(21)   End if
(22)   End For
(23)     t = t + 1
(24)  End While
(25)  End Differential Evolution
```

Pseudocode 1

4. Numerical Results and Discussions

The simulation results are drawn to compare the performance of the proposed and existing schemes in sidelobe concealments of the NC-OFDM symbol. This section discusses five different cases, i.e., one spectral hole, multiple spectral holes, SUs with equal bandwidth distribution, PUs with equal bandwidth distribution, and PUs and SUs with unequal bandwidth distribution as in Table 1. The DE algorithm performance is analyzed with a population size of 100 with a total of 800 iterations and random selection of the base vector. The scaling factor is tuned at 0.2 for local minimum. The crossover rate is binomial and fixed as 0.9. The total number of cancellation carriers in the CC technique

Table 1: Simulation parameters.

Parameter	Case 1	Case 2	Case 3	Case 4	Case 5
Hole availability	One	Four holes with equal SU and PU regions	Four holes with equal SUs regions	Four holes with equal PU regions	Four holes with unequal PUs and SUs regions
Population size	100	100	100	100	100
Iterations	800	800	800	800	800
Scaling factor	0.2	0.2	0.2	0.2	0.2
Subcarriers in each hole	16	16	16	35, 15, 40, 20	45, 20, 25, 30
Extra subcarriers in the CC technique	2	2	2	2	2

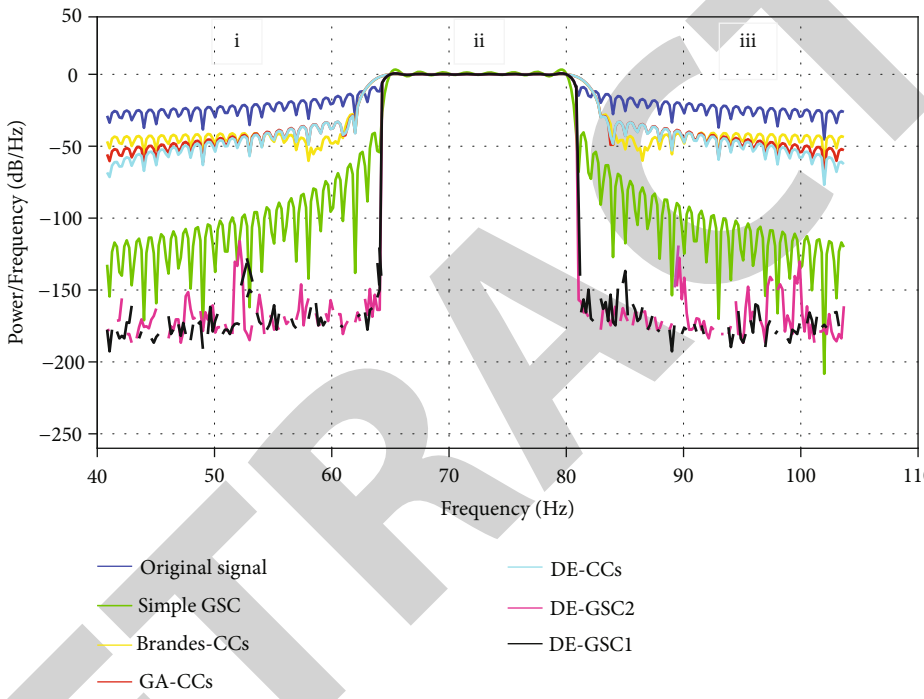

Figure 4: PSD of the original signal, simple GSC, DE-GSC2, DE-GSC1, Brandes-CCs, GA-CCs, and DE-CCs in case 1.

is 2. Simulation results of the proposed DE-GSC1 and DE-GSC2 along with simple GSC, Brandes-CCs, GA-CCs, and DE-CCs are shown in the form of normalized power spectral density (PSD) in Figures 4–8.

4.1. Case 1: Single White Space and Two Equal PU Bands. In the first case, three subbands are considered with single whitespace available for the SUs. In Figure 4, regions (i) and (iii) are available for the PU, whereas region (ii) is occupied by the SUs dynamically. A total of 16 subcarriers is considered in this case that is further modulated with the BPSK modulation. The PSD of the NC-OFDM signal on all its subcarriers is normalized to 1. The results are compared with some existing techniques such as (1) CCs on NC-OFDM signal for clampdown of sidelobes [17], (2) optimized CCs using DE algorithm with GA [9], and (3) sidelobe suppression using simple GSC in [22]. Figure 4 shows that the proposed DE-GSC1 and DE-GSC2 can effectively reduce unwanted sidelobes in PU regions (i) and (iii) as compared with the original signal, simple GSC, Brandes-CC, DE-CC, and GA-CC techniques.

A comparison of the proposed and other schemes is further elaborated in Table 2, which reveals the sidelobes' power in the PU regions. The results in Figure 4 and Table 2 show that the original signal has a sidelobe power of -28 dB and -27 dB in regions (i) and (iii). It is clear from Table 2 that the GSC scheme reduces sidelobes' power in both regions to -131 dB and -132 dB. Similarly, the Brandes-CC results show a reduction in the sidelobes' power in regions (i) and (iii) to -48 dB each. Sidelobe power in the GA-CCs is lowered to -56 dB in region (i) and -55 dB in region (iii), while the DE-CCs further reduce that to -64 dB in region (i) and -66 dB in region (iii). The sidelobe power minimization ability is almost similar to the traditional Brandes-CCs, GA-CCs, and DE-CCs in regions (i) and (iii). A significant reduction in the sidelobes' power is

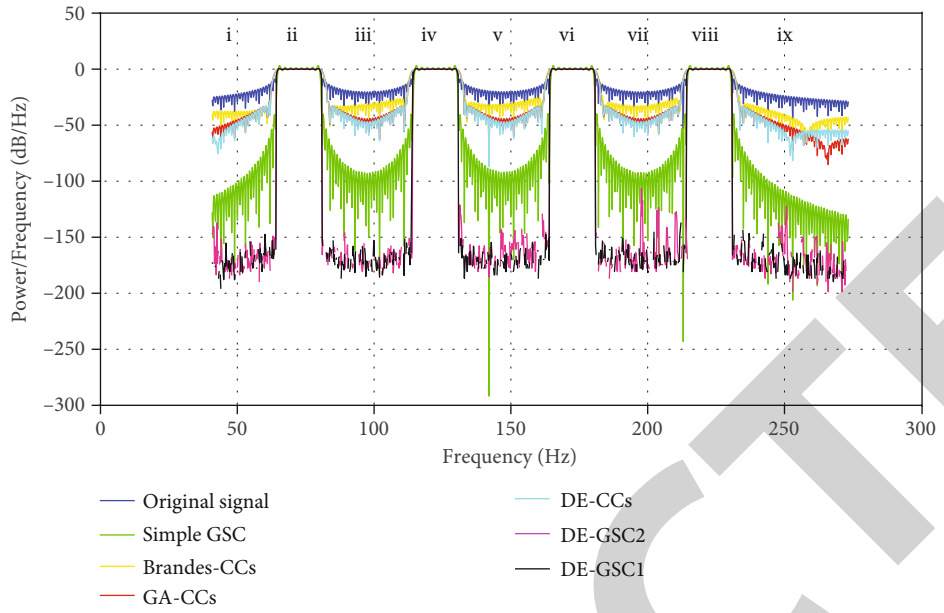

Figure 5: PSD of the original signal, simple GSC, DE-GSC2, DE-GSC1, Brandes-CCs, GA-CCs, and DE-CCs in case 2.

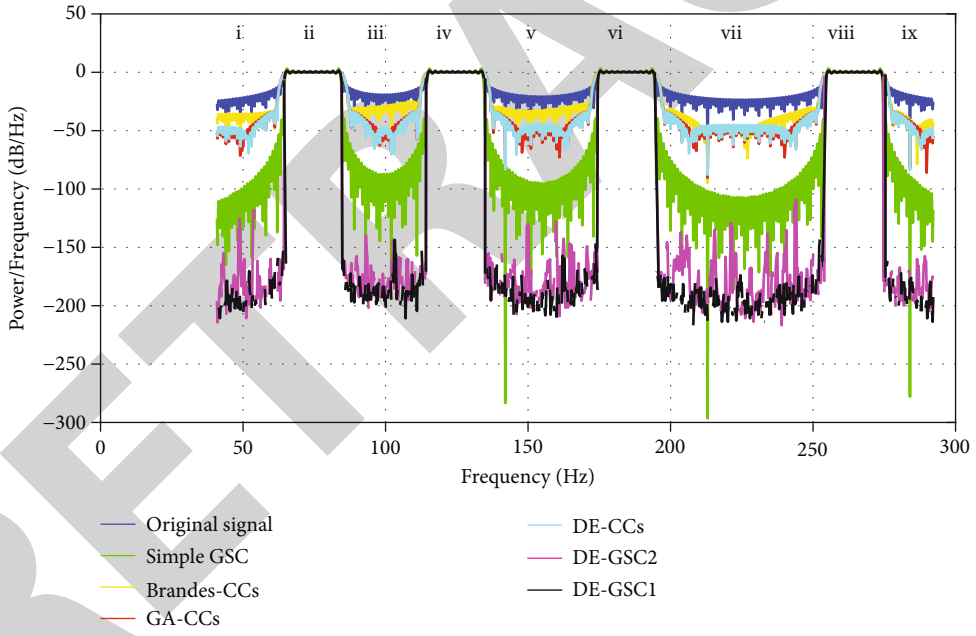

Figure 6: PSD of the original signal, simple GSC, DE-GSC2, DE-GSC1, Brandes-CCs, GA-CCs, and DE-CCs in case 3.

observable when the proposed DE-GSC1 and DE-GSC2 schemes are practiced in the given scenario. The results obtained by the proposed DE-GSC1 are -175 dB in region (i) and -173 dB in region (iii). Similarly, the proposed DE-GSC2 reduces sidelobes' power to -153 dB in region (i) and -155 dB in the region (iii). Hence, the proposed schemes can reduce sidelobes' powers significantly as compared with simple GSC, DE-CC, GA-CC, and Brandes-CC techniques.

4.2. Case 2: Four Equal White Spaces and Five Equal PU Bands. In this case, the spectrum is divided into multiple subbands with four white spaces for the SUs and five PU bands. The available bandwidth is distributed between PUs and SUs, as follows: spaces (i), (iii), (v), (vii), and (ix) are available for the PU, whereas regions (ii), (iv), (vi), and (viii) are occupied by SUs. The total number of subcarriers used by the SUs in case 2 is 16 which are modulated using the BPSK modulation. Figure 5 shows that the DE-GSC1 and DE-GSC2 considerably reduce the sidelobe power in PU regions (i), (iii), (v), (vii), and (ix) as compared with the simple GSC, DE-CC, GA-CC, and Brandes-CC techniques.

Table 3 shows the numerical values of the resultant sidelobes power in five PU regions (i), (iii), (v), (vii), and (ix).

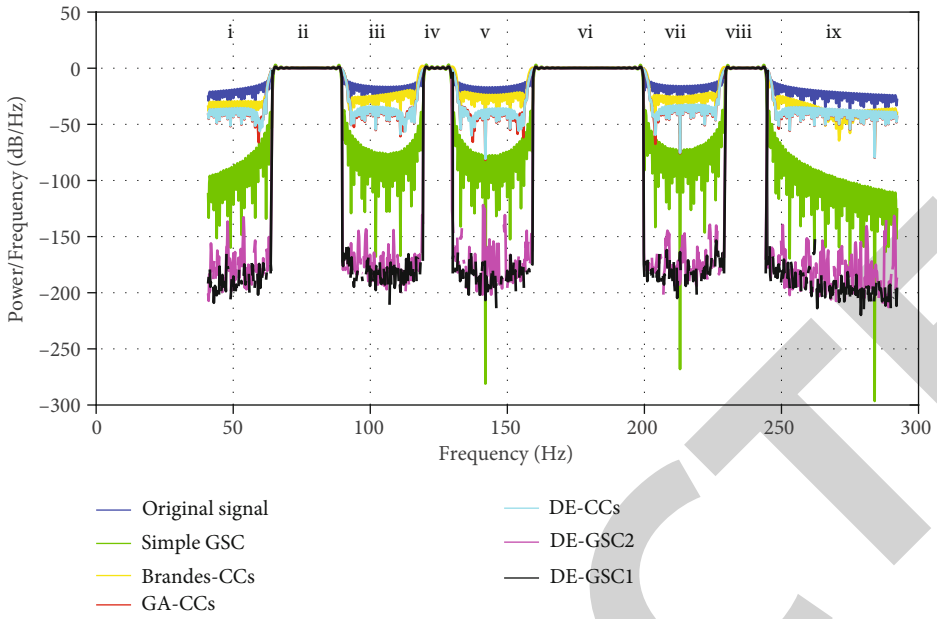

Figure 7: PSD of the original signal, simple GSC, DE-GSC2, DE-GSC1, Brandes-CCs, GA-CCs, and DE-CCs in case 4.

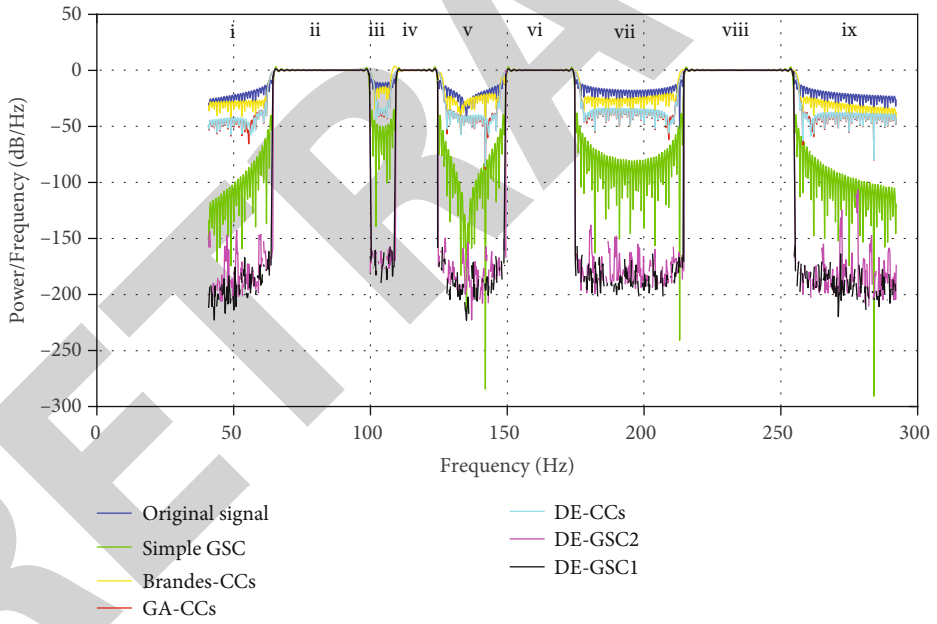

Figure 8: PSD of the original signal, simple GSC, DE-GSC2, DE-GSC1, Brandes-CCs, GA-CCs, and DE-CCs in case 5.

These results show that the original signal has an average sidelobe power of -24.8 dB that is reduced by the Brandes-CCs to an average of -48.8 dB. The average sidelobe results of the GA-CCs and DE-CCs are -64.8db and -52.2 dB, while the simple GSC average power is -134.6 dB. Similarly, the proposed DE-GSC1 and DE-GSC2 schemes can reduce sidelobe power to an average of -165.4 dB and -159.8 dB in these regions.

4.3. Case 3: Four Equal White Spaces and Five Unequal PU Bands. In the third case, the spectrum is divided into multiple subbands. The bandgap of PUs in this case is unequal, i.e., regions (i), (iii), (v), (vii), and (ix), whereas SU regions (ii), (iv), (vi), and (viii) are of equal bandwidth. The total subcarriers utilized at the SUs, in this case, are 16. BPSK modulation is followed to modulate these subcarriers. In Figure 6 and Table 4, the comparison between the proposed and existing schemes is shown. The results obtained for the proposed DE-GSC1 and DE-GSC2 have the lowest sidelobe power among all the other schemes in the case of unequal spectrum regions (i), (iii), (v), (vii), and (ix).

Table 2: Sidelobe power in case 1.

Techniques	Sidelobe power in PU locations i	iii
Original signal	-28 dB	-27 dB
Simple GSC	-132 dB	-131 dB
Brandes-CCs	-48 dB	-48 dB
GA-CCs	-56 dB	-55 dB
DE-CCs	-64 dB	-66 dB
DE-GSC1	-175 dB	-173 dB
DE-GSC2	-153 dB	-155 dB

Table 3: Sidelobe power in case 2.

Techniques	Sidelobe power in PU locations i	iii	v	vii	ix
Original signal	-26 dB	-23 dB	-23 dB	-26 dB	-26 dB
Simple GSC	-130 dB	-135 dB	-136 dB	-136 dB	-136 dB
CC-Brandes	-48 dB	-49 dB	-49 dB	-49 dB	-49 dB
CC-GA	-56 dB	-54 dB	-51 dB	-50 dB	-50 dB
CC-DE	-64 dB	-65 dB	-65 dB	-65 dB	-65 dB
DE-GSC1	-170 dB	-168 dB	-164 dB	-162 dB	-163 dB
DE-GSC2	-155 dB	-165 dB	-162 dB	-155 dB	-162 dB

Table 4: Sidelobe power in case 3.

Techniques	Sidelobe power in PU locations i	iii	v	vii	ix
Original signal	-32 dB	-29 dB	-28 dB	-27 dB	-28 dB
Simple GSC	-130 dB	-132 dB	-134 dB	-135 dB	-136 dB
Brandes-CCs	-40 dB	-42 dB	-43 dB	-44 dB	-45 dB
GA-CCs	-50 dB	-52 dB	-51 dB	-50 dB	-50 dB
DE-CCs	-51 dB	-53 dB	-52 dB	-53 dB	-54 dB
DE-GSC1	-180 dB	-175 dB	-178 dB	-179 dB	-177 dB
DE-GSC2	-160 dB	-158 dB	-161 dB	-160 dB	-157 dB

Table 5: Sidelobe power in case 4.

Techniques	Sidelobe power in PU locations i	iii	v	vii	ix
Original signal	-26 dB	-25 dB	-24 dB	-25 dB	-26 dB
Simple GSC	-136 dB	-137 dB	-138 dB	-133 dB	-137 dB
Brandes-CCs	-48 dB	-48 dB	-47 dB	-46 dB	-48 dB
GA-CCs	-56 dB	-54 dB	-53B	-53 dB	-53 dB
DE-CCs	-64 dB	-65 dB	-62 dB	-64 dB	-66 dB
DE-GSC1	-178 dB	-177 dB	-176 dB	-175 dB	-176 dB
DE-GSC2	-165 dB	-163 dB	-165 dB	-166 dB	-164 dB

Table 4 shows numerical results of the sidelobe powers in case 3 for the proposed and other schemes. It is noticeable that the proposed DE-GSC1 while reducing sidelobe power is the most suitable scheme under unequal band gaps occupied by the PU. It is clear from Table 4 that the original signal has an average sidelobe power of -28.8 dB that is reduced by the Brandes-CCs to an average of -42.8 dB. The DE-CC and GA-CC average suppression results are -52.6 dB and -50.6 dB, while the simple GSC average suppression results are -133.4 dB. The DE-GSC1 and DE-GSC2 average suppression results in the PU regions are -177.8 dB and -159.2 dB.

Table 6: Sidelobe power in case 5.

Techniques	Sidelobe power in PU locations i	iii	v	vii	ix
Original signal	-24 dB	-26 dB	-23 dB	-26 dB	-26 dB
Simple GSC	-136 dB	-135 dB	-136 dB	-130 dB	-133 dB
Brandes-CCs	-48 dB	-47 dB	-45 dB	-47 dB	-49 dB
GA-CCs	-52 dB	-50 dB	-51 dB	-50 dB	-50 dB
DE-CCs	-66 dB	-65 dB	-67 dB	-66 dB	-64 dB
DE-GSC1	-179 dB	-178 dB	-176 dB	-172 dB	-173 dB
DE-GSC2	-160 dB	-161 dB	-162 dB	-159 dB	-162 dB

4.4. Case 4: Four Unequal White Spaces and Five Equal PU Bands. In this case, the SUs have unequal band gap distribution, while the PUs have an equal band gap distribution. Here, regions (ii), (iv), (vi), and (viii) are occupied by SU as illustrated in Figure 7, and regions (i), (iii), (v), (vii), and (ix) are occupied by PUs. The total subcarriers used at the SU's regions are 35, 15, 40, and 20, respectively. The results in Figure 7 show that the proposed DE-GSC1 and DE-GSC2 efficiently reduce sidelobes' powers in the PU equal regions, i.e., (i), (iii), (v), (vii), and (ix).

The original signal in Table 5 has the average sidelobe power of -25.2 dB that is reduced by the Brandes-CCs to an average of -47.4 dB. The GA-CCs and DE-CCs can suppress more and reduce sidelobe power to an average result of -53.8 dB and -64.2 dB. Similarly, the simple GSC suppression results are -136.2 dB, while the proposed DE-GSC1 and DE-GSC2 schemes have -164.6 dB and -176.4 dB on average.

4.5. Case 5: Four Unequal White Spaces and Five Unequal PU Bands. A multiple subband with unequal SUs and PUs bandgap allocation is discussed in case 5. Unequal bandgap regions (ii), (iv), (vi), and (viii) are allotted to the SUs. However, regions (i), (iii), (v), (vii), and (ix) are occupied by the PUs. The total numbers of subcarriers at the SUs are 45, 20, 25, and 30, respectively.

Figure 8 shows that the proposed DE-GSC1 and DE-GSC2 have better sidelobe reduction as compared with the simple GSC, Brandes-CCs, GA-CCs, and DE-CCs. The numerical results of the sidelobe power are shown in Table 6. It is clear from the results that the original signal average sidelobe power is -25 dB which is reduced by the Brandes-CCs to an average of -47.2 dB. The GA-CC and DE-CC average suppression results are -50.6 dB and -65.6 dB. The simple GSC results in better performance than the CC techniques while achieving an average of -134 dB. Both the proposed DE-GSC1 and DE-GSC2 dominate the schemes with better average suppression results of -175.6 dB and -160.8 dB.

Hence, it can be concluded from the above comparison that both the proposed DE-GSC1 and DE-GSC2 schemes performed better than the simple GSC, GA-CCs, DE-CCs, and Brandes-CCs in various scenarios and produce high accuracy to reduce sidelobe power in the PU locations.

5. Conclusion

The use of the NC-OFDM scheme in the free spectral hole has a sidelobe issue that results in interference in the legitimate PU regions. In this paper, a sufficiently large number of sidelobe sample points are taken into consideration for optimization using the DE algorithm in the DE-GSC1. The DE algorithm determines a suitable adaptive weight vector for the GSC that results in efficient reduction of the sidelobes issues in the PU region. However, the DE-GSC2 takes the initial sample points in the sidelobe region near the main NC-OFDM signal and determines the remaining points utilizing the sidelobes decay function. The different cases discussed in the paper show superiority of the proposed schemes to efficiently access the available spectrum holes without hindering the PU transmission. The results confirmed a significant reduction in the sidelobe interference by following the proposed scheme as compared with the existing techniques.

As the GSC has been examined widely in radar and communication systems where the desired signal needs to be measured either in time or at the amplitude level, it is suggested that a dual function radar and communication system can be designed by controlling the main lobe for radar and sidelobes for the communication systems employing the DE-based GSC approach, presented in this paper.

In a future work, we intend to reconfigure the adaptive vector of the GSC while utilizing machine learning techniques aiming to improve interference suppression. Furthermore, time and computational complexity analysis will be carried out to compare with existing interference minimization schemes such as optimization-based CCs and GSC.

Data Availability

The data used to support the findings of this study are included in the article.

Disclosure

This work was funded and supported in part by the National Research Foundation of Korea (NRF) grant funded by the Korean Government (MSIT) (Nos. 2016R1C1B1014069 and 2021R1A2C1013150).

Conflicts of Interest

The authors declare no conflict of interest.

References

[1] P. Kolodzy, "Spectrum policy task force: findings and recommendations," *Federal Communications Commission*, vol. 2, no. 35, pp. 1–14, 2003.

[2] N. Gul, I. M. Qureshi, S. Akbar, M. Kamran, and I. Rasool, "One-to-many relationship based Kullback Leibler divergence against malicious users in cooperative spectrum sensing," *Wireless Communications and Mobile Computing*, vol. 2018, 14 pages, 2018.

[3] A. Patel, M. Z. Khan, S. N. Marchant, U. B. Desai, and L. Hanzo, "The achievable rate of interweave cognitive radio in the face of sensing errors," *IEEE Access*, vol. 5, pp. 8579–8605, 2017.

[4] T. Renk, C. Kloeck, and F. K. Jondral, "A cognitive approach to the detection of spectrum holes in wireless networks," in *4th IEEE Consumer Communications and Networking Conference*, pp. 1118–1120, Las Vegas, NV, USA, 2007.

[5] X. Hong, C. X. Wang, H. H. Chen, and Y. Zhang, "Secondary spectrum access networks," *IEEE Vehicular Technology Magazine*, vol. 4, no. 2, pp. 36–43, 2009.

[6] N. Gul, I. M. Qureshi, A. Naveed, A. Elahi, and I. Rasool, "Secured soft combination schemes against malicious-users in cooperative spectrum sensing," *Wireless Personal Communications*, vol. 108, no. 1, pp. 389–408, 2019.

[7] N. Gul, I. M. Qureshi, A. Omar, A. Elahi, and S. Khan, "History based forward and feedback mechanism in cooperative spectrum sensing including malicious users in cognitive radio network," *PLoS One*, vol. 12, no. 8, pp. 1–21, 2017.

[8] N. Gul, I. M. Qureshi, A. Elahi, and I. Rasool, "Defense against malicious users in cooperative spectrum sensing using genetic algorithm," *International Journal of Antennas and Propagation*, vol. 2018, 11 pages, 2018.

[9] A. Elahi, I. M. Qureshi, F. Zaman, and F. Munir, "Reduction of out of band radiation in non-contiguous OFDM based cognitive radio system using heuristic techniques," *Journal of Information Science and Engineering*, vol. 32, pp. 349–364, 2016.

[10] R. W. Chang, "Synthesis of band-limited orthogonal signals for multichannel data transmission," *Bell System Technical Journal*, vol. 45, no. 10, pp. 1538–1966, 1966.

[11] G. M. Abdalla, "Orthogonal frequency division multiplexing theory and challenges," *Khartoum University Engineering Journal*, vol. 1, no. 2, pp. 1–8, 2011.

[12] B. Farhang-Boroujeng and R. Kempter, "Multicarrier communication techniques for spectrum sensing and communication in cognitive radios," *IEEE Communication Magazine*, vol. 46, no. 4, pp. 80–85, 2008.

[13] H. A. Mahmoud and H. Arslan, "Sidelobe suppression in OFDM-based spectrum sharing systems using adaptive symbol transition," *IEEE Communications Letters Magazine*, vol. 12, no. 2, pp. 133–135, 2008.

[14] D. Noguet, M. Gautier, and V. Berg, "Advances in opportunistic radio technologies for TVWS," *EURASIP Journal on Wireless Communications and Networking (JWCN)*, vol. 2011, no. 1, pp. 1–12, 2011.

[15] T. Weiss, J. Hillenbrand, A. Krohn, and F. K. Jondral, "Mutual interference in OFDM-based spectrum pooling systems," in *2004 IEEE 59th vehicular technology conference. VTC 2004-Spring*, pp. 118–1877, Milan, Italy, 2005.

[16] A. Sahin and H. Arslan, "Edge windowing for OFDM based systems," *IEEE Communications Letters*, vol. 15, no. 11, pp. 1208–1211, 2011.

[17] S. Brandes, I. Cosovic, and M. Schenell, "Reduction of out-of-band radiation in OFDM systems by insertion of cancellation carriers," *IEEE Communications Letters*, vol. 10, no. 6, pp. 420–422, 2006.

[18] I. Cosovic, S. Brandes, and M. Schnell, "Subcarrier weighting: a method for sidelobe suppression in OFDM systems," *IEEE Communications Letters*, vol. 10, no. 6, pp. 444–446, 2006.

[19] A. Selim, I. Macaluso, and L. Doyle, "Efficient sidelobe suppression for OFDM systems using advanced cancellation carriers," in *2013 IEEE International Conference on Communications (ICC)*, pp. 4687–4692, Budapest, Hungary, 2013.

[20] K. Bisht and S. Tyagi, "Subcarrier weighting sidelobe suppression technique for OFDM based cognitive radio systems," *International Journal on Emerging Technologies*, vol. 8, pp. 117–120, 2017.

[21] A. Selim, B. Orgul, and L. Doyle, "Efficient sidelobe suppression for OFDM systems with peak-to-average power ratio reduction," in *2012 IEEE International Symposium on Dynamic Spectrum Access Networks*, pp. 510–516, Bellevue, WA, USA, 2012.

[22] A. Elahi, I. M. Qureshi, Z. Khan, and F. Zaman, "Sidelobe reduction in non-contiguous ofdm-based cognitive radio systems using a generalized sidelobe canceller," *Applied Sciences.*, vol. 5, no. 4, pp. 894–909, 2015.

[23] I. C. Viel and T. Mazzoni, "Sidelobe suppression in OFDM spectrum sharing systems via additive signal method," in *IEEE Vehicular Technology Conference*, pp. 2692–2696, Dublin, Ireland, 2007.

[24] D. Qu, Z. Wang, and T. Jiang, "Extended active interference cancellation for sidelobe suppression in cognitive radio OFDM systems with cyclic prefix," *IEEE Transactions on Vehicular Technology*, vol. 59, no. 4, pp. 2692–2696, 2010.

[25] R. Ahmed, A. Elahi, G. Ahmed, and N. Gul, "Sidelobe minimization in orthogonal frequency division multiplexing using efficient generalize sidelobe canceler," in *17th International Bhurban Conference on Applied Sciences and Technology (IBCAST)*, pp. 674–678, Islamabad, Pakistan, 2020.

[26] R. Ahmed, A. Elahi, N. Gul, and S. Khan, "Minimization of out of band radiations in orthogonal frequency division multiplexing using modified generalize sidelobe canceler," in *2019 International Conference on Electrical, Communication, and Computer Engineering*, pp. 1–5, Swat, Pakistan, 2019.

[27] A. Elahi, A. Ahmed, N. Gul, R. Ahmed, and M. Kamran, "A mongrel technique for the reduction of sidelobes in ofdm – based cognitive radio system," in *2020 17th International Bhurban Conference on Applied Sciences and Technology (IBCAST*, pp. 686–689, Islamabad, Pakistan, 2020.

[28] A. Kaleem, S. Haq, A. Elahi, and N. Gul, "Minimization of OOB radiation in OFDM based cognitive radio system using multiple GSC," in *2019 International Conference on Electrical, Communication, and Computer Engineering (ICECCE)*, pp. 1–5, Swat, Pakistan, 2019.

[29] A. I. Zaki, A. A. Hendy, W. K. Badawi, and E. F. Badran, "Joint PAPR reduction and sidelobe suppression in NC-OFDM based cognitive radio using wavelet packet and SC techniques," *Physical Communication*, vol. 35, no. 2, p. 100695, 2019.

[30] H. Yuan, E. Li, and F. Zeng, "Filter design for suppressing sidelobe interference in NC-OFDM system," *International Symposium on Communication Engineering & Computer Science (CECS)*, vol. 86, pp. 72–77, 2018.

[31] K. Sravan-Kumar, K. Sahitya, and K. Nama-Naidu, "A hybrid technique for joint PAPR reduction and sidelobe suppression in NC- OFDM based cognitive radio systems," *AEU-International Journal of Electronics Communications*, vol. 100, pp. 172–178, 2019.

[32] S. Dikmese, A. Loulou, S. Srinivasan, and M. Renfors, "Spectrum sensing and resource allocation models for enhanced OFDM based cognitive radio," in *9th International Conference on Cognitive Radio Oriented Wireless Networks and Communications (CROWNCOM)*, pp. 360–365, Oulu, Finland, 2014.

[33] H. L. Van-Trees, "Optimum array processing," in *Optimum Array Processing*, John Wiley & Sons, 2002.

[34] P. Vergallo, "Processing EEG signals through beamforming techniques for seizure diagnosis," in *2012 Sixth International Conference on Sensing Technology (ICST)*, pp. 497–501, Kolkata,India, 2012.